Copy 212
RM E53I23

NACA

RESEARCH MEMORANDUM

PERFORMANCE OF SEPARATION NOSE INLETS AT MACH NUMBER 5.5

By Rudolph C. Haefeli and Harry Bernstein

Lewis Flight Propulsion Laboratory
Cleveland, Ohio

NATIONAL ADVISORY COMMITTEE
FOR AERONAUTICS

WASHINGTON
December 1, 1953

NACA RM E53I23 [redacted]

NATIONAL ADVISORY COMMITTEE FOR AERONAUTICS

RESEARCH MEMORANDUM

PERFORMANCE OF SEPARATION NOSE INLETS AT MACH NUMBER 5.5

By Rudolph C. Haefeli and Harry Bernstein

SUMMARY

Two nose inlets utilizing the boundary-layer separation ahead of a blunt body to provide a compression surface have been tested at a Mach number of 5.5 and a Reynolds number based on model diameter of 427,000. At zero angle of attack, a maximum total-pressure recovery of 13.8 percent, corresponding to a kinetic-energy efficiency of 87.4 percent, was obtained for the spherical-nose inlet; and a maximum recovery of 10.7 percent, corresponding to an efficiency of 85.2 percent, was obtained for the planar-nose inlet. The mass-flow ratios at maximum recovery were 0.91 and 1.00, respectively. At an angle of attack of 3°, a maximum recovery of 4 percent was obtained, corresponding to an efficiency of 75.1 percent. The mass-flow ratio was 0.50. For the configurations which yielded these maximum recoveries, the flow was unstable during subcritical operation.

INTRODUCTION

Supersonic nose inlets may require blunt-nose centerbodies in order to accommodate guidance equipment. For minimizing the blunt-body drag and for efficient external compression, the boundary-layer separation occurring on a prong projecting upstream of the blunt body has been utilized (refs. 1 and 2). The boundary of the separated-flow region acts as the external compression surface of the inlet and effectively simulates the solid cone of a single-conical-shock nose inlet, at least at zero angle of attack. Some important aspects of this flow separation phenomenon are discussed in references 3, 4, and 5.

As a continuation of investigations of the performance of various types of nose inlets at a Mach number of approximately 5.5 (ref. 6), two separation inlets have been tested in the NACA Lewis 6- by 6-inch tunnel. For one of these the diffuser forebody had a spherical nose, whereas for the other the blunt body had a planar nose normal to the stream-flow direction. The results of these tests are reported herein.

[redacted]

SYMBOLS

The following symbols are used in this report:

D	diameter of cowl at inlet entrance
M	Mach number
m	mass-flow rate
P	total pressure
γ	ratio of specific heats, 1.4 for air
η_{KE}	kinetic-energy efficiency, $\frac{\text{kinetic energy of air expanded isentropically from diffuser exit to free-stream static pressure}}{\text{free-stream kinetic energy}}$

Subscripts:

0	free-stream tube of diameter D
1	combustion-chamber conditions

APPARATUS

The tests were conducted in the Lewis 6- by 6-inch continuous-flow hypersonic tunnel at a nominal Mach number of 5.5. The test-section total pressure was between 86.5 and 89.0 pounds per square inch absolute, with a variation of ±0.5 pound per square inch during any one run. The stagnation temperature was 233±8° F. These inlet conditions were sufficient to avoid condensation of the air components, as evidenced by use of the light scattering technique described in reference 7. The test-section Reynolds number, based on an average total pressure of 87.5 pounds per square inch absolute and on the maximum model diameter, was 427,000.

The separation inlets are shown in figures 1 and 2. The spherical nose (figs. 1(a) and 2(a)) had a radius of 0.63 inch; the sphere was tangent to a cone of 27° half-angle at the inlet entrance station. The planar-nose forebody (figs. 1(b) and 2(b)) consisted of a truncated cone of 27° half-angle. The forward section of this forebody was made of six

removable plates of 0.06-inch thickness. The location of the face of the forebody relative to the cowl could be changed by removing one or more of these plates. Shims of various thickness were inserted between the centerbody and each of the forebodies (figs. 1(c) and 2(a)) to change the location of the nose relative to the cowl. This also changed the internal geometry of the inlets. Each of the inlets was equipped with a variable-length prong of 0.250-inch diameter. Three conical prong tips with the following dimensions were used:

Tip	Cone half-angle, deg	Length, in.	Diameter, in.
1	20	0.50	0.250
2	20	.68	.375
3	27	.40	.250

The cowl and internal contour of these inlets were the same as those of the inlet described in reference 6.

The instrumentation for measuring combustion-chamber pressures is shown in figures 1(c) and 2(a). The seven pitot-pressure probes were made from 0.050-inch outside-diameter steel tubing with the opening flattened to inside dimensions of 0.002 by 0.040 inch. The six static-pressure orifices had diameters of 0.021 inch. The pressures were read on a mercury manometer.

The pitot- and static-pressure probes described in reference 8 were used to determine the free-stream conditions. The pitot and static pressures were measured with mercury and butyl phthalate manometers, respectively.

Schlieren photographs of the flow about the model were obtained using an exposure time of about 2 microseconds.

REDUCTION OF DATA

The results of a Mach number survey at an axial station $33\frac{3}{4}$ inches downstream of the tunnel throat are presented in figure 3. The model was located with the leading edge of its cowl at a station $36\frac{1}{2}$ inches from the tunnel throat. The Mach numbers, determined by use of the Rayleigh equation from pitot and static pressure measurements, were reproducible within 2 percent. Inasmuch as the variations from Mach number 5.5, indicated in figure 3, are generally within the reproducibility, a nominal Mach number of 5.5 was chosen for computations of diffuser performance.

The test-section pitot pressure was measured at locations approximately 1 inch ahead of the cowl leading-edge station after each model test. The free-stream total pressure was computed from these measurements and from the normal-shock relation for a Mach number of 5.5.

The pressure recoveries of the inlet were based on an arithmetic average of the seven pitot-pressure readings in the combustion chamber. This method of averaging was believed to be sufficiently accurate as differences between the seven pressures were in most cases less than 1/2 inch of mercury, which represents, at peak recovery, a deviation from the mean of less than 1½ percent of its value. Because of the unsymmetrical location of the pitot tubes with the model at angle of attack, the pressures were measured at both positive and negative values of the same angle and the 14 pitot pressures were averaged in the computation of the pressure recovery. For this method, the probable error in the maximum recovery is estimated to be about 1 percent of its value.

The diffuser mass-flow ratio was based on the average of the six combustion-chamber static-pressure readings (twelve readings at angle of attack) and on a Mach number computed from the ratio of the effective minimum exit area to the combustion-chamber area. The single-conical-shock inlet (with cone retracted 0.01 in.) of reference 6 was used to calibrate the outlet plug, as this inlet operates at a mass-flow ratio of unity throughout the supercritical range. This calibration provided a factor which was applied to the geometric outlet area to obtain the effective area. In the subcritical range the correction factor was assumed to have the same value as at critical operation. A check on this method of mass-flow ratio computation (ref. 6) showed it to be satisfactory.

RESULTS AND DISCUSSION

For each configuration the prong length was adjusted at the beginning of each run to be in the range for minimum mass-flow spillage indicated by schlieren observations. Minor adjustments were then made to obtain the length for maximum total-pressure recovery. The diffuser characteristics to be presented were obtained with this optimum prong length, unless otherwise noted. The prong lengths were restricted in the present tests to those for which separation occurred at the shoulder, because data presented in references 1 and 2 show that larger recoveries can be obtained with this condition than with the separation point on the prong cylinder.

Spherical-Nose Inlet

Effect of prong tip geometry. - An initial test was performed with the spherical nose to determine the effect of changes in the geometry of

the prong tip. The total-pressure recovery and mass-flow ratio obtained with three tips are shown in figure 4. For this test the forebody was in its original design position relative to the cowl, that is, no shim was used between the forebody and the centerbody. The maximum total-pressure recovery, 11.6 percent, was obtained with the 27°, 1/4-inch-diameter tip (tip 3). Inasmuch as the tip geometry did not have much effect on performance in this test, only tips 2 and 3 were employed in subsequent tests.

The maximum pressure recoveries were obtained over a relatively large range of mass-flow ratios under conditions of stable operation (fig. 4). Although larger recoveries were obtained, as will be shown, for other locations of the nose relative to the cowl, the subcritical flow was then unstable.

Schlieren photographs of the inlet operating near maximum recovery with each of the tips are presented in figure 5. Because the separated flow boundary does not meet the spherical nose tangentially, an oblique shock originates on the sphere ahead of the inlet entrance. This shock provides external compression in addition to the compression behind the shock originating at the prong tip. Thus the shock pattern of the separation inlet is similar to that of a two-shock conical-nose inlet. The present shock configuration, however, permits flow spillage in front of the cowl.

Effect of nose position and prong length. - In figure 6 the effect of changing the position of the nose relative to the cowl is shown for prong tips 2 and 3. For each nose location, data are presented for the prong length which yielded the largest total-pressure recovery, except for the configuration with prong length 0.966 D (fig. 6(a)). The largest recovery indicated on the figures for each configuration is the maximum that could be obtained. The greatest recoveries were obtained with the nose moved forward from its design position. With tip 2 (fig. 6(a)), the maximum recovery was 0.130 at a mass-flow ratio of 0.90, for which the nose was 0.056 inch forward of its design position and the prong length was 0.834 D. With tip 3 (fig. 6(b)), the maximum recovery was 0.138 at a mass-flow ratio of 0.91, for which the shim thickness was 0.040 inch and the prong length was 0.715 D. The performance curve for the inlet with the 0.107 inch shim indicates the large losses in recovery and mass flow incurred by moving the nose too far forward.

The kinetic-energy efficiencies corresponding to the maximum pressure recoveries obtained with tips 2 and 3, as determined from the equation

$$\eta_{KE} = 1 - \frac{\left(\frac{P_0}{P_1}\right)^{\frac{\gamma-1}{\gamma}} - 1}{\frac{\gamma-1}{2} M_0^2}$$

were 87.0 percent and 87.4 percent, respectively.

Schlieren photographs which illustrate typical shock configurations and separated flow regions for stable flow are presented in figure 7. Figures 7(a) and 7(b) illustrate the flow patterns for tip 2 and tip 3 with the shim thicknesses and prong lengths which gave maximum recovery.

Data are presented in figure 6(a) for the inlet with a 0.056-inch shim and a prong length of 0.966 D, which is 0.132 D longer than required for optimum recovery. The greatest recovery obtained with the longer prong is about 14 percent less than the optimum recovery of 0.130. This decrease represents a 1 percent loss in kinetic-energy efficiency. A schlieren photograph of the inlet with the longer prong (fig. 7(c)) shows that the shock wave originating on the spherical nose enters the inlet. Also, there is a pronounced curvature of the separated-flow boundary and of the conical tip shock. This indicates that the lesser recovery results because the Mach number of the flow entering the inlet is greater than that for the geometry of figure 7(a), so that the pressure loss across the shocks within the inlet is greater.

For some configurations, the curves of figure 6 are extended into the unstable flow region. The data points for the unstable flow represent time-average values; the pressures appeared constant on the manometers because of inertia of the manometer system. Schlieren photographs typical of these unstable flows are shown in figure 8. The tip shock oscillates between a position corresponding to stable flow and a position far ahead of the entire inlet.

Angle of attack performance. - At an angle of attack of 3° the performance of the spherical-nose inlet (fig. 9) was poor. With the best configuration the maximum total-pressure recovery was only 4 percent and the maximum mass-flow ratio was only 0.5. This recovery is the same as the pressure recovery through a normal shock at a Mach number of 5.6 and corresponds to a kinetic-energy efficiency of 75.1 percent. Operation could not be extended into the stable region any farther than shown because the maximum combustion-chamber outlet area was limited by the size of the exit flow annulus. The mass-flow ratio, however, cannot be expected to increase much beyond its value at peak recovery.

Poor angle of attack performance has been previously noted for separation inlets at lower Mach numbers in references 1 and 2. The loss

in pressure recovery and mass flow at angle of attack is due to the cross-flow velocity components which enlarge the separated region on the low-pressure side of the prong (fig. 10). Excessive flow spillage therefore occurs on that side of the inlet. The performance at angle of attack can be substantially improved, however, by alining the prong with the stream direction at each angle of attack. This has been demonstrated in the investigation of reference 2.

Planar-Nose Inlet

The planar-nose inlet was tested with all the forebody plates installed, and with two plates removed from the upstream end. It was also tested with all the plates and with a 0.056 inch shim. The performance for each of these configurations is shown in figure 11, and schlieren photographs of the flow are presented in figure 12. The maximum total-pressure recovery, obtained at a mass-flow ratio of 1.0, was 10.7 percent, which corresponds to an efficiency of 85.2 percent.

The performance of the inlet with one plate removed was about the same as with two plates removed. With all the forebody plates removed, the inlet did not start, since the separated region covered the entire inlet face. At angle of attack the performance of the planar-nose inlet was as poor as that of the spherical-nose inlet.

Some Operating Characteristics

With the spherical forebody moved forward of its original design position and with the planar-nose forebody, the inlet flow was unstable when the outlet area was reduced beyond the area for maximum recovery. In general, stable flow could not be reestablished by increasing the outlet area only; it was also necessary to change the prong length. After the stable flow was reestablished the prong length could be readjusted to the value for maximum recovery.

Rapid fluctuations of the separated flow boundary and the shock wave originating at the prong tip occurred during supercritical operation of the inlets. The magnitude of these fluctuations is indicated by the schlieren photographs in figure 13. The fluctuations did not occur during a run at a flow Reynolds number of 1.48×10^6 based on model diameter, which indicates that they are due to instability of the separated flow at the test Reynolds number.

Comparison with Single-Conical-Shock Inlet

The performance of the separation inlets is compared with the performance of a single-conical-shock nose inlet in figure 14. The conical-nose inlet, which is the same inlet discussed in reference 6, was operated

with the cone retracted 0.01 inch from its original design location and with silicon carbide grit on the cone tip. The performance of this inlet under the conditions of the present investigation differs from that in reference 6 because the Mach number and stream total-pressure were larger for the present data. The separation inlet data pertain to the geometric configurations (variables are shim thickness and prong length) for which maximum recoveries were obtained. The zero angle of attack performance of the separation inlets is comparable with that of the single-conical-shock inlet. At angle of attack, however, the separation inlets exhibited much poorer pressure recoveries and mass-flow ratios.

3041

SUMMARY OF RESULTS

Two nose inlets utilizing the boundary-layer separation ahead of a blunt body to provide a compression surface were tested at a Mach number of 5.5 and a Reynolds number based on model diameter of 427,000. For one of these inlets the centerbody nose was spherical, whereas for the other the nose was planar in a direction normal to the stream. The maximum total-pressure recovery, the corresponding kinetic-energy efficiency, and the mass-flow ratio at maximum recovery are summarized in the following table for each inlet. Corresponding data for a single-conical shock nose inlet are presented for comparison.

Forebody	Angle of attack, deg	Maximum total-pressure recovery	Kinetic-energy efficiency, percent	Mass-flow ratio at peak recovery
Spherical	0	0.138	87.4	0.91
Planar	0	.107	85.2	1.00
Conical	0	.123	86.4	1.00
Spherical	3	.040	75.1	.50
Conical	3	.114	85.8	.95

For the configurations which yielded these data, the flow was unstable during subcritical operation.

Lewis Flight Propulsion Laboratory
National Advisory Committee for Aeronautics
Cleveland, Ohio, September 30, 1953

REFERENCES

1. Moeckel, W. E., and Evans, P. J., Jr.: Preliminary Investigation of Use of Conical Flow Separation for Efficient Supersonic Diffusion. NACA RM E51J08, 1951.

2. Hearth, Donald P., and Gorton, Gerald C.: Investigation at Supersonic Speeds of an Inlet Employing Conical Flow Separation from a Probe Ahead of a Blunt Body. NACA RM E52K18, 1953.

3. Mair, W. A.: Experiments on Separation of Boundary Layers on Probes in Front of Blunt-Nosed Bodies in a Supersonic Air Stream. Phil. Mag., vol. 43, no. 342, July 1952, pp. 695-716.

4. Jones, Jim J.: Flow Separation from Rods Ahead of Blunt Noses at Mach Number 2.72. NACA RM L52E05a, 1952.

5. Moeckel, W. E.: Flow Separation Ahead of a Blunt Axially Symmetric Body at Mach Numbers 1.76 to 2.10. NACA RM E51I25, 1951.

6. Bernstein, Harry, and Haefeli, Rudolph C.: Investigation of Pressure Recovery of a Single-Conical-Shock Nose Inlet at Mach Number 5.4 NACA RM E53A12, 1953.

7. Hansen, C. Frederick, and Nothwang, George J.: Condensation of Air in Supersonic Wind Tunnels and its Effect on Flow about Models. NACA TN 2690, 1952.

8. Haefeli, Rudolph C.: Use of Fences to Increase Uniformity of Boundary Layer on Side Walls of Supersonic Wind Tunnels. NACA RM E52E19, 1952.

(a) Spherical-forebody inlet.

Figure 1. - Separation inlets mounted in Lewis 6- by 6-inch hypersonic tunnel.

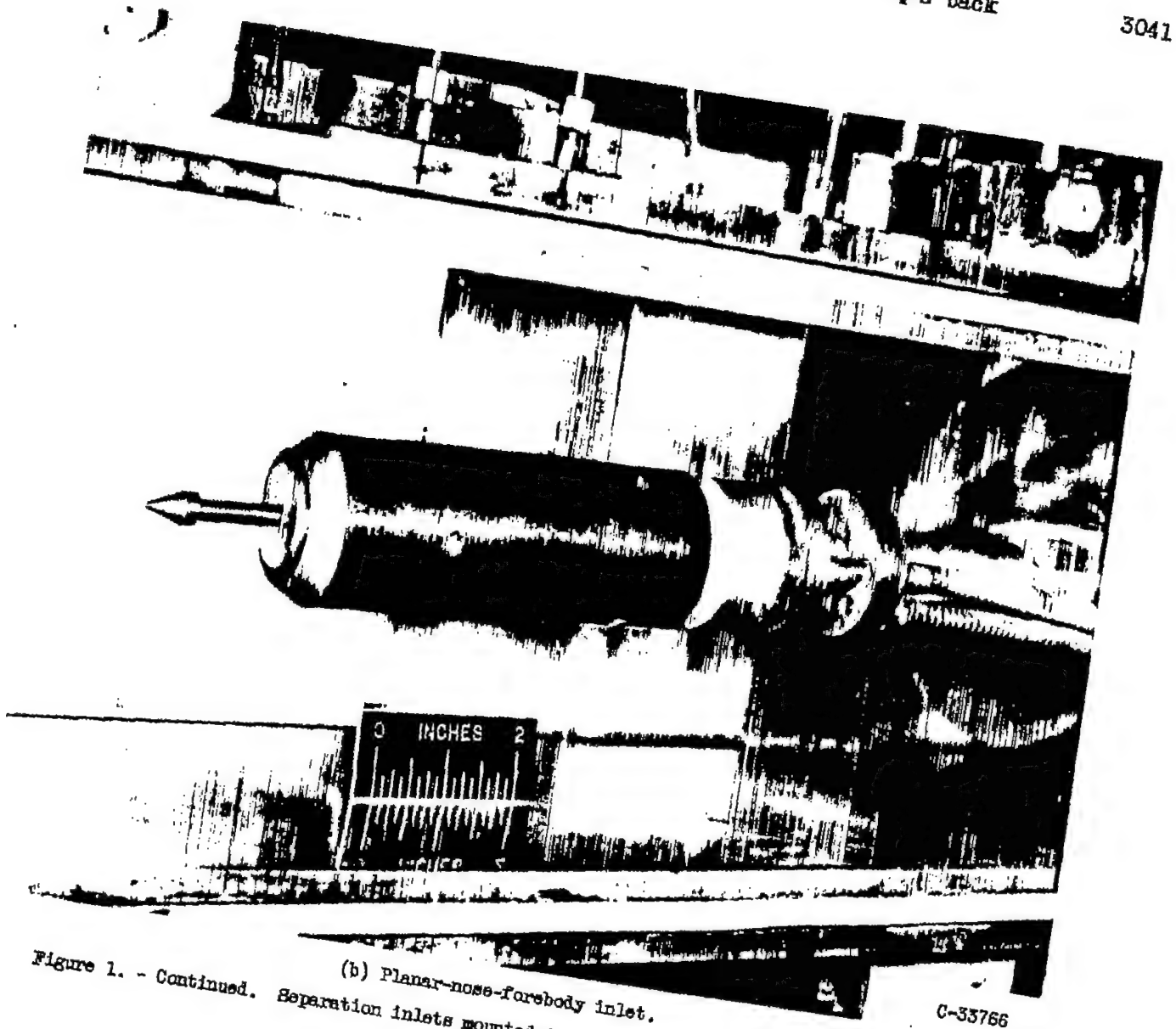

(b) Planar-nose-forebody inlet. C-33766

Figure 1. - Continued. Separation inlets mounted in Lewis 6- by 6-inch hypersonic tunnel.

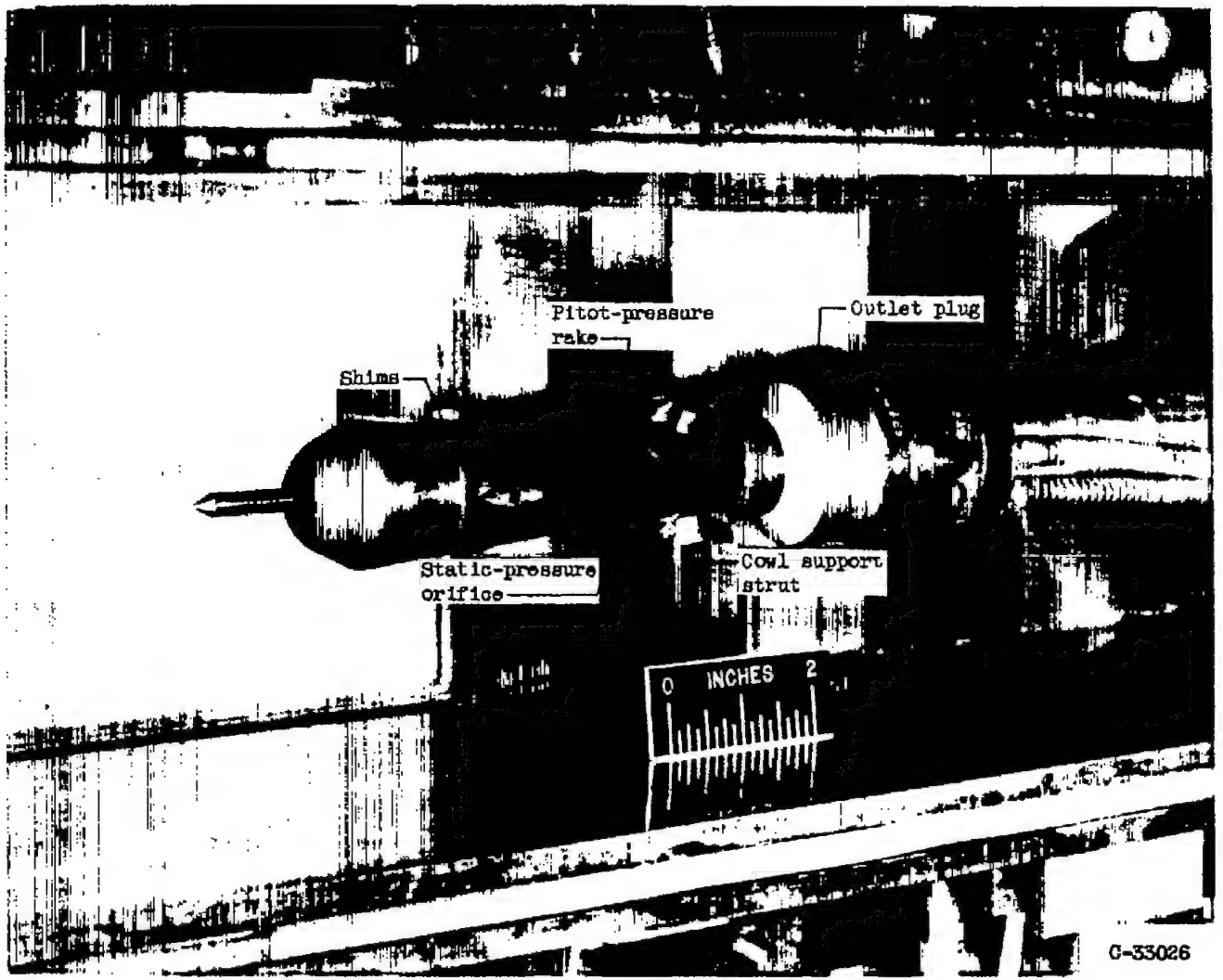

(c) Spherical-forebody inlet with cowl removed to show instrumentation.

Figure 1. - Concluded. Separation inlets mounted in Lewis 6- by 6-inch hypersonic tunnel.

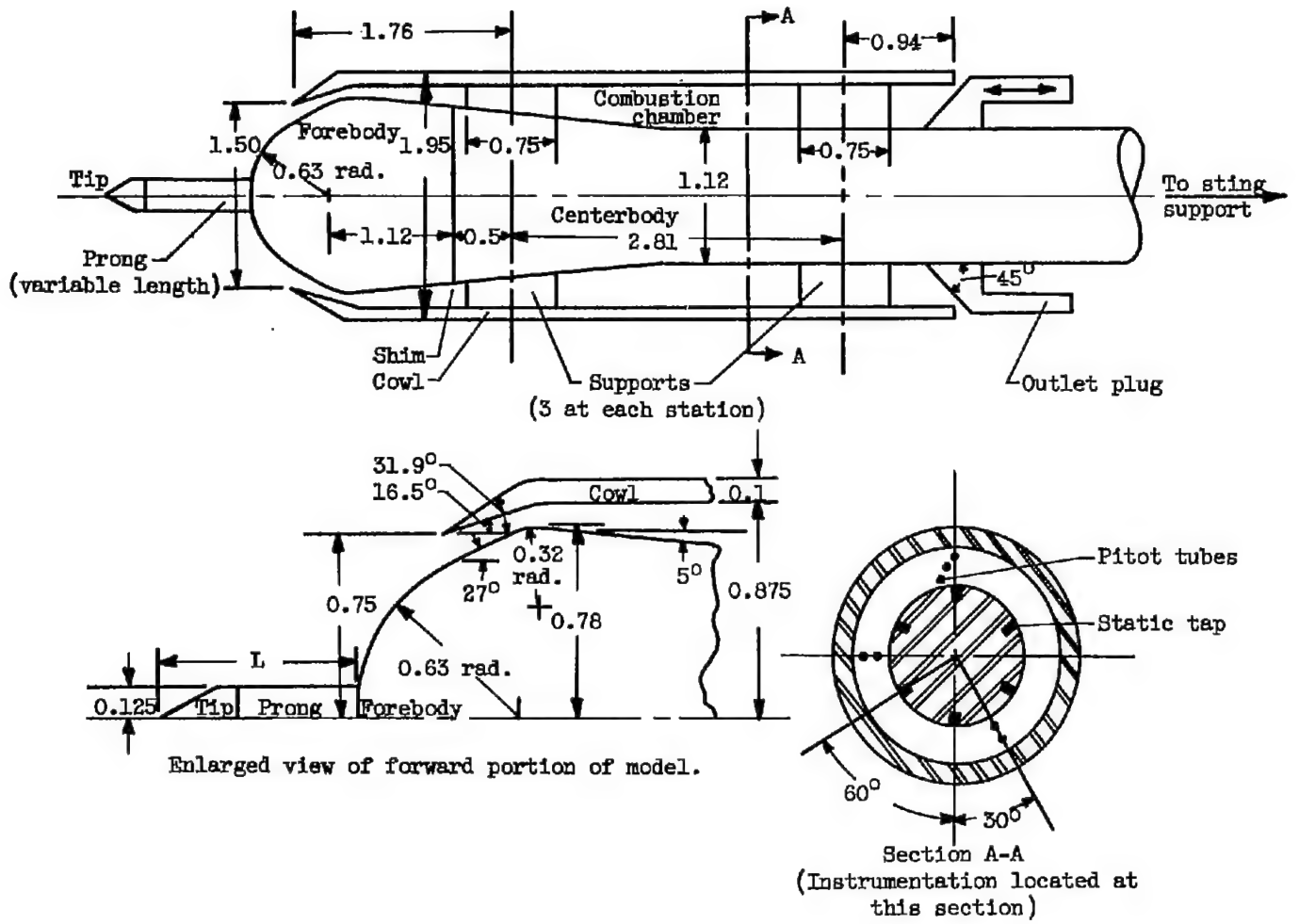

(a) Spherical-forebody inlet.

Figure 2. - Separation inlets showing dimensions and location of instrumentation. (All dimensions are in inches.)

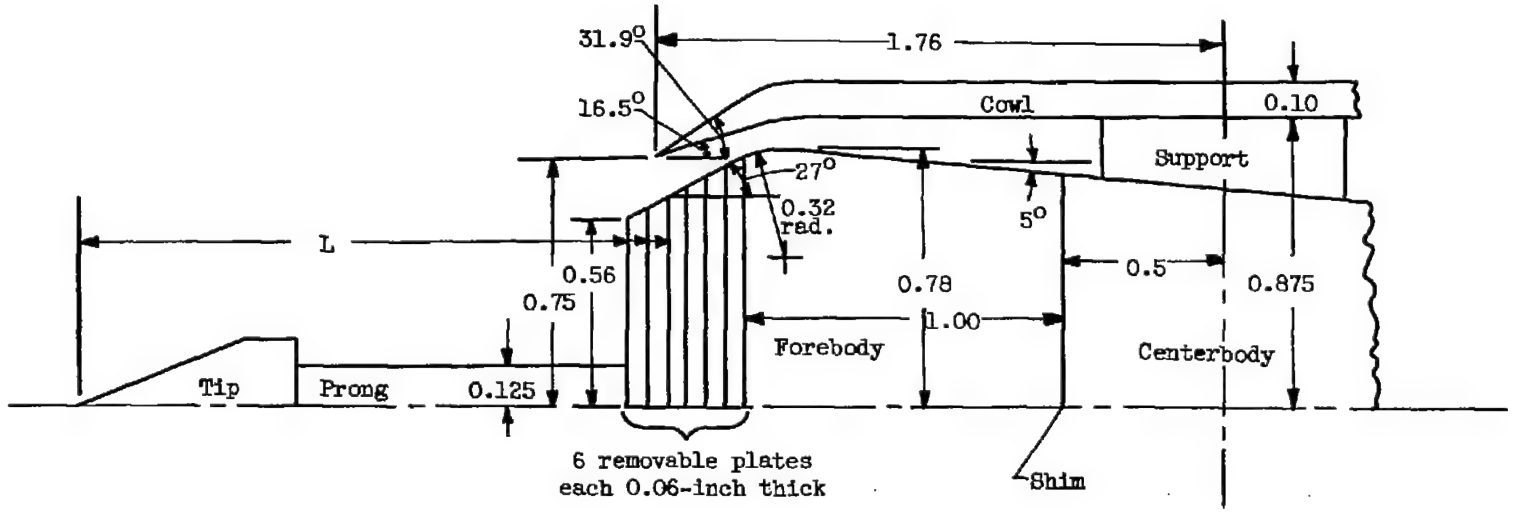

(b) Planar-forebody inlet.

Figure 2. - Concluded. Separation inlets showing dimensions and location of instrumentation. (All dimensions are in inches.)

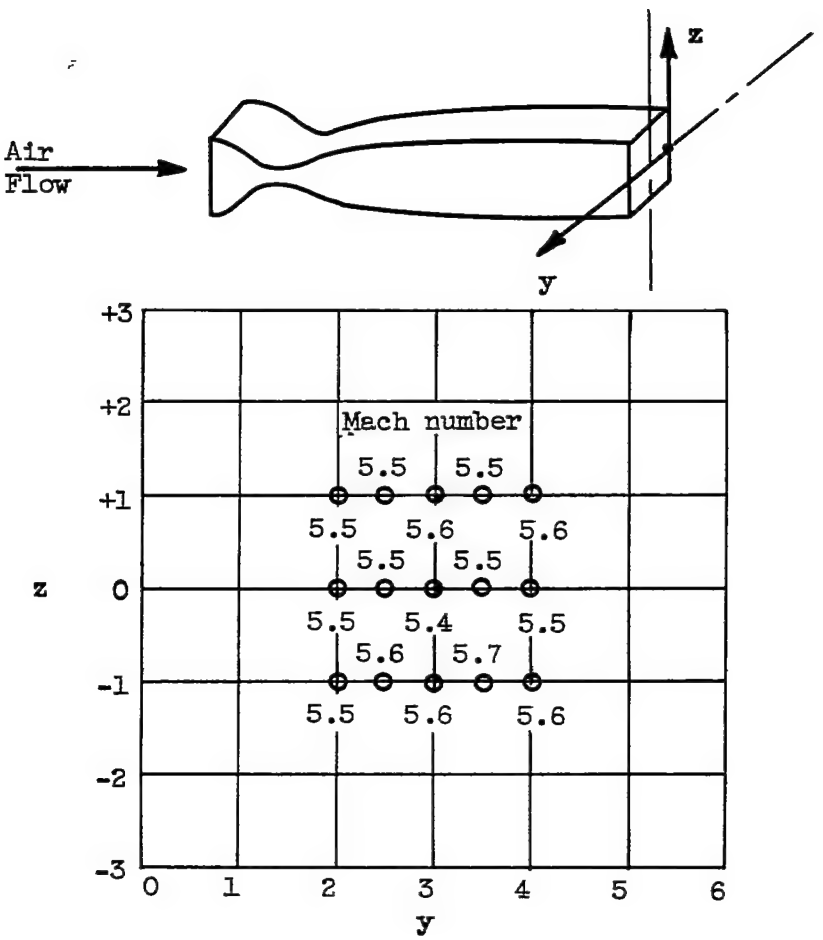

Figure 3. - Mach number calibration $33\frac{3}{4}$ inches downstream of throat of Lewis 6- by 6-inch hypersonic tunnel.

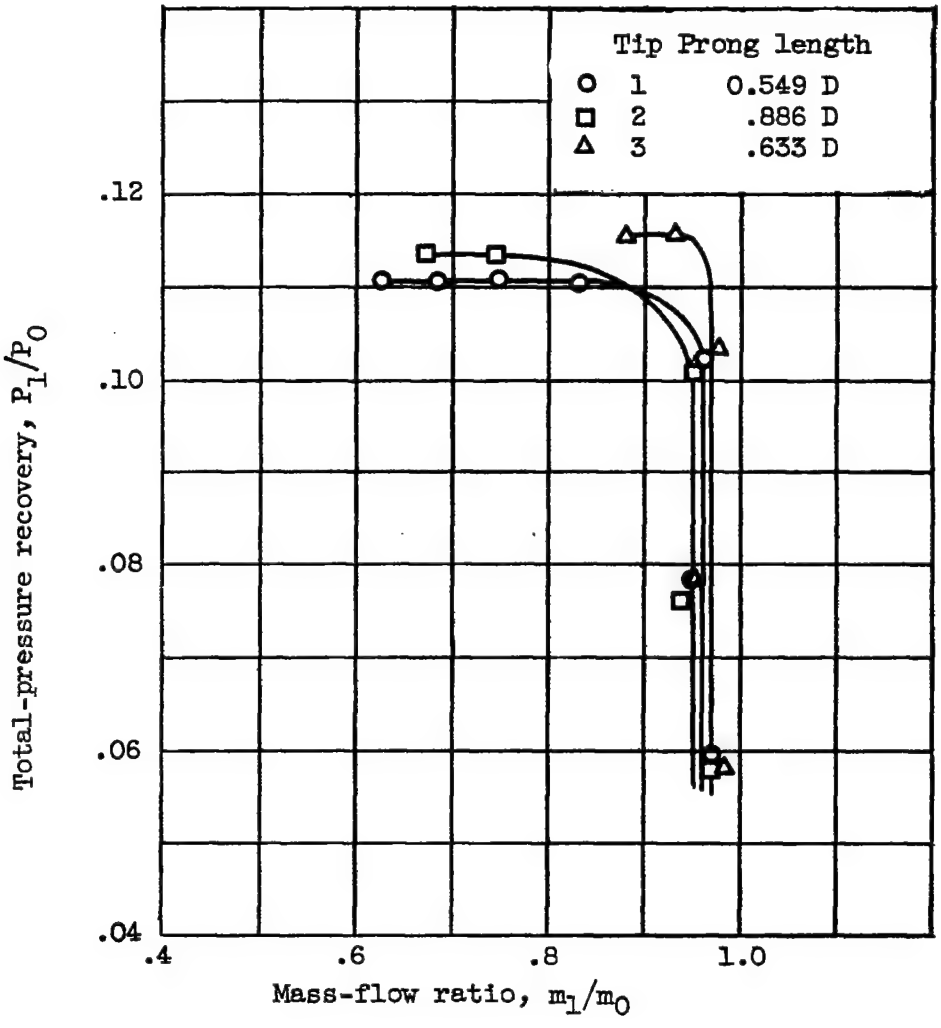

Figure 4. - Diffuser characteristics with various prong tips. Spherical nose; no shim; zero angle of attack.

(a) Tip 1; prong length, 0.549 D.

(b) Tip 2; prong length, 0.886 D.

(c) Tip 3; prong length, 0.633 D.

Figure 5. - Schlieren photographs of diffuser with three tip configurations. Spherical nose; no shim; zero angle of attack.

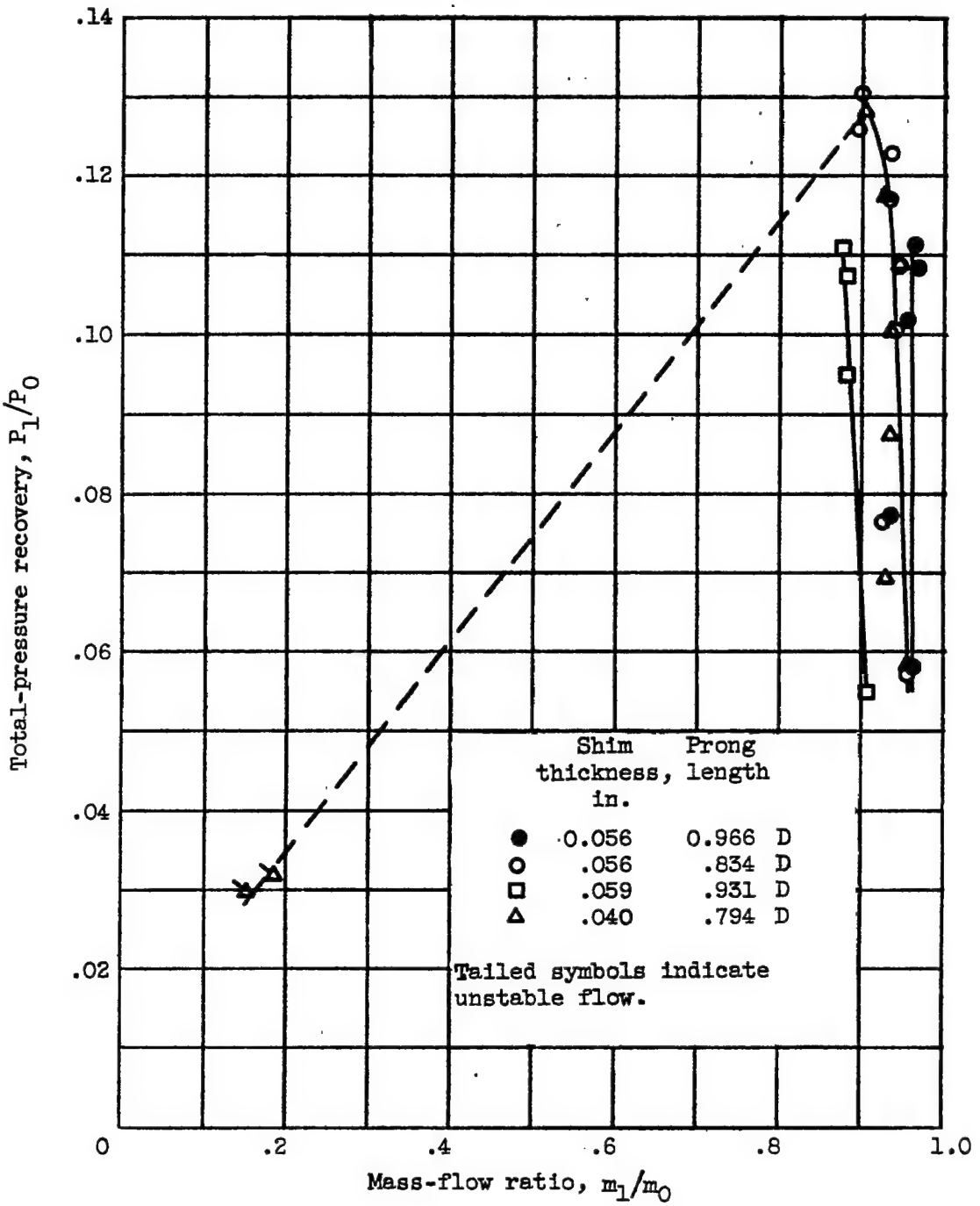

(a) Tip 2.

Figure 6. - Diffuser characteristics showing effects of shim thickness and prong length. Spherical nose; zero angle of attack.

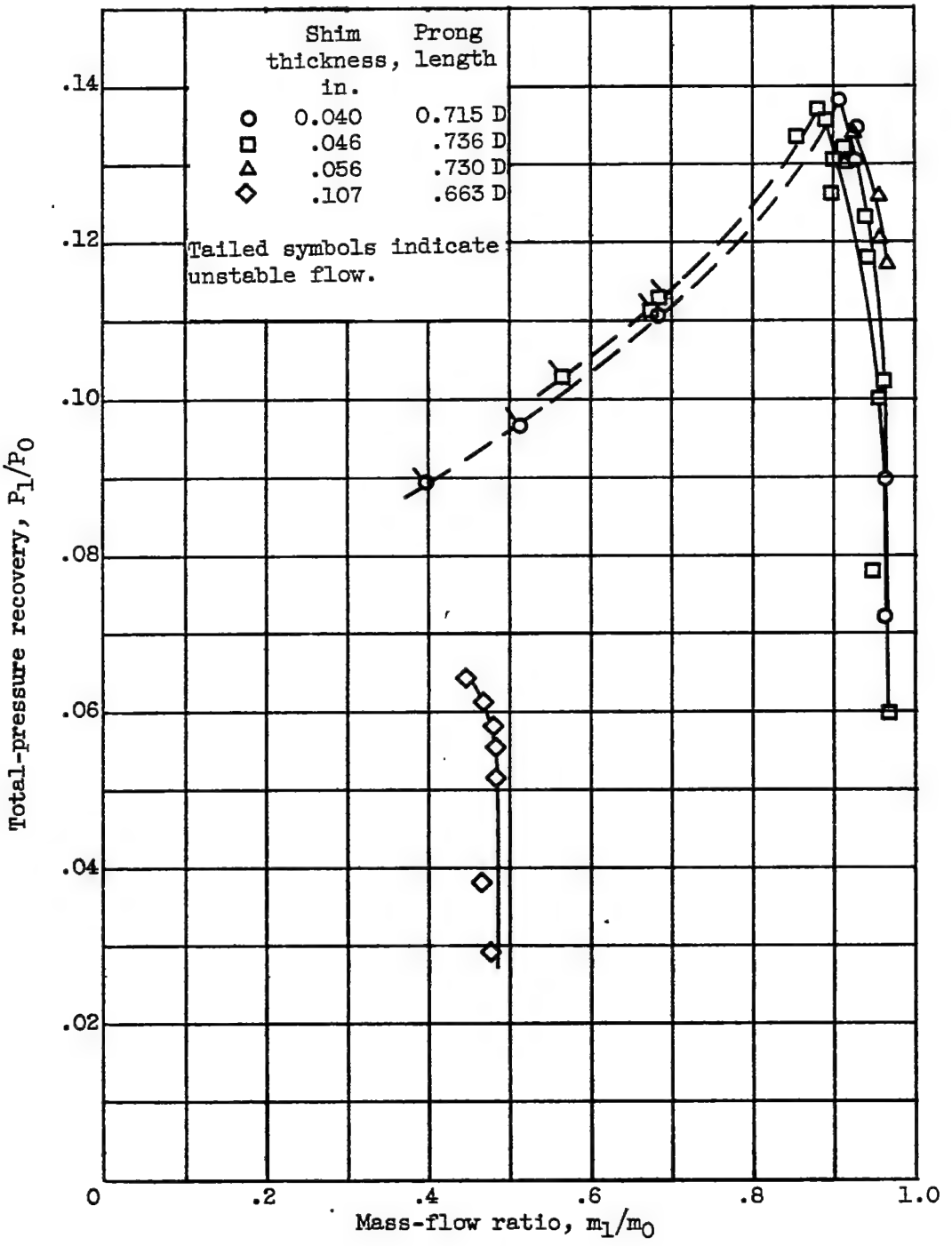

(b) Tip 3.

Figure 6. - Concluded. Diffuser characteristics showing effects of shim thickness and prong length. Spherical nose; zero angle of attack.

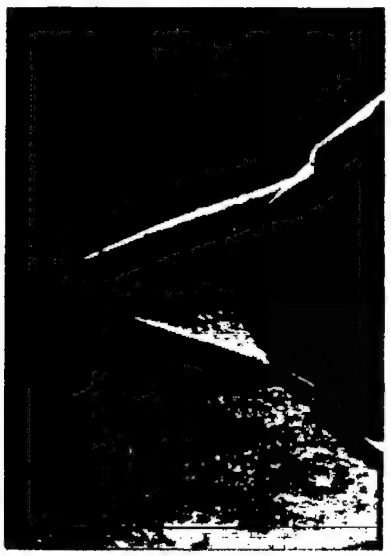

(a) Tip 2; shim thickness, 0.056 inch; prong length, 0.834 D.

(b) Tip 3; shim thickness, 0.040 inch; prong length, 0.715 D.

(c) Tip 2; shim thickness, 0.056 inch; prong length, 0.966 D.

Figure 7. - Schlieren photographs of diffuser at zero angle of attack. Stable flow; spherical nose.

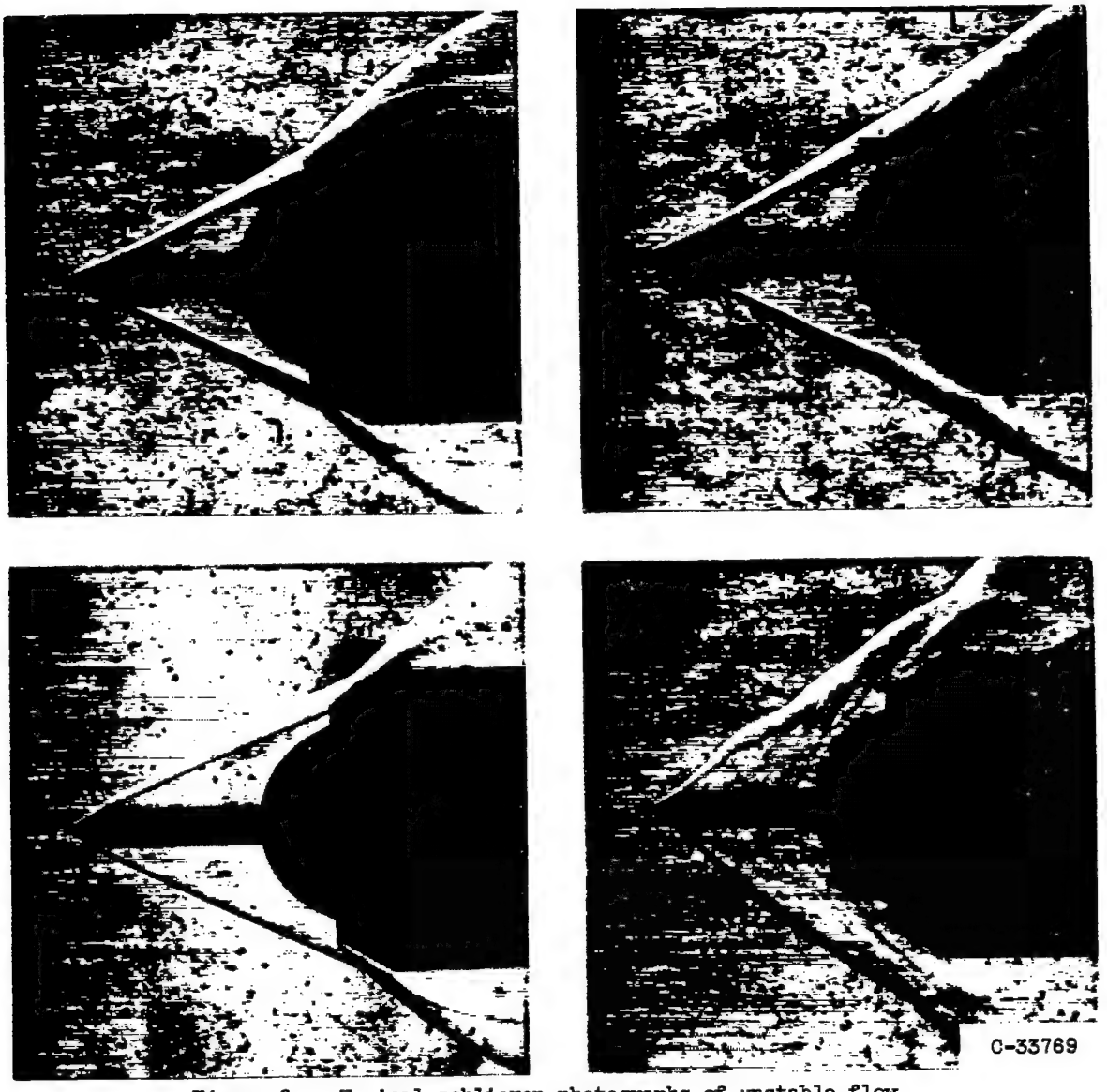

Figure 8. - Typical schlieren photographs of unstable flow.

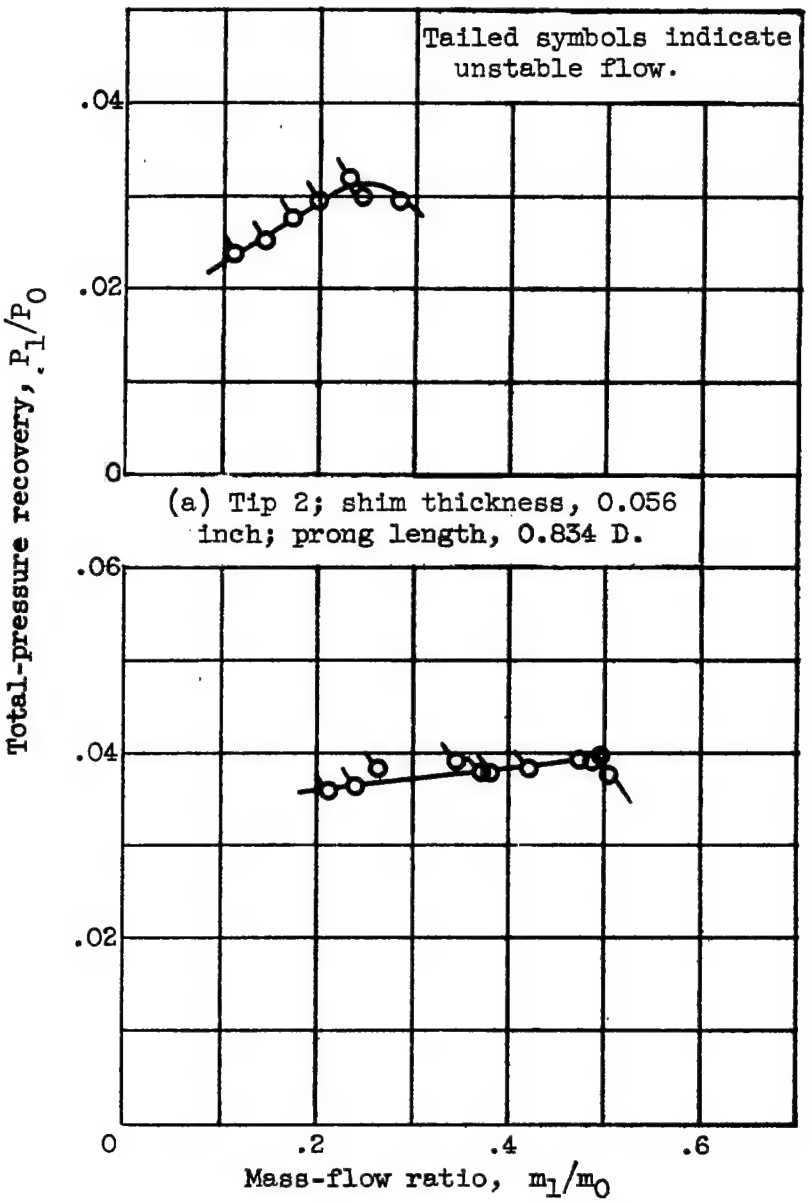

(b) Tip 3; shim thickness, 0.046 inch; prong length, 0.736 D.

Figure 9. - Diffuser performance at 3° angle of attack. Spherical nose.

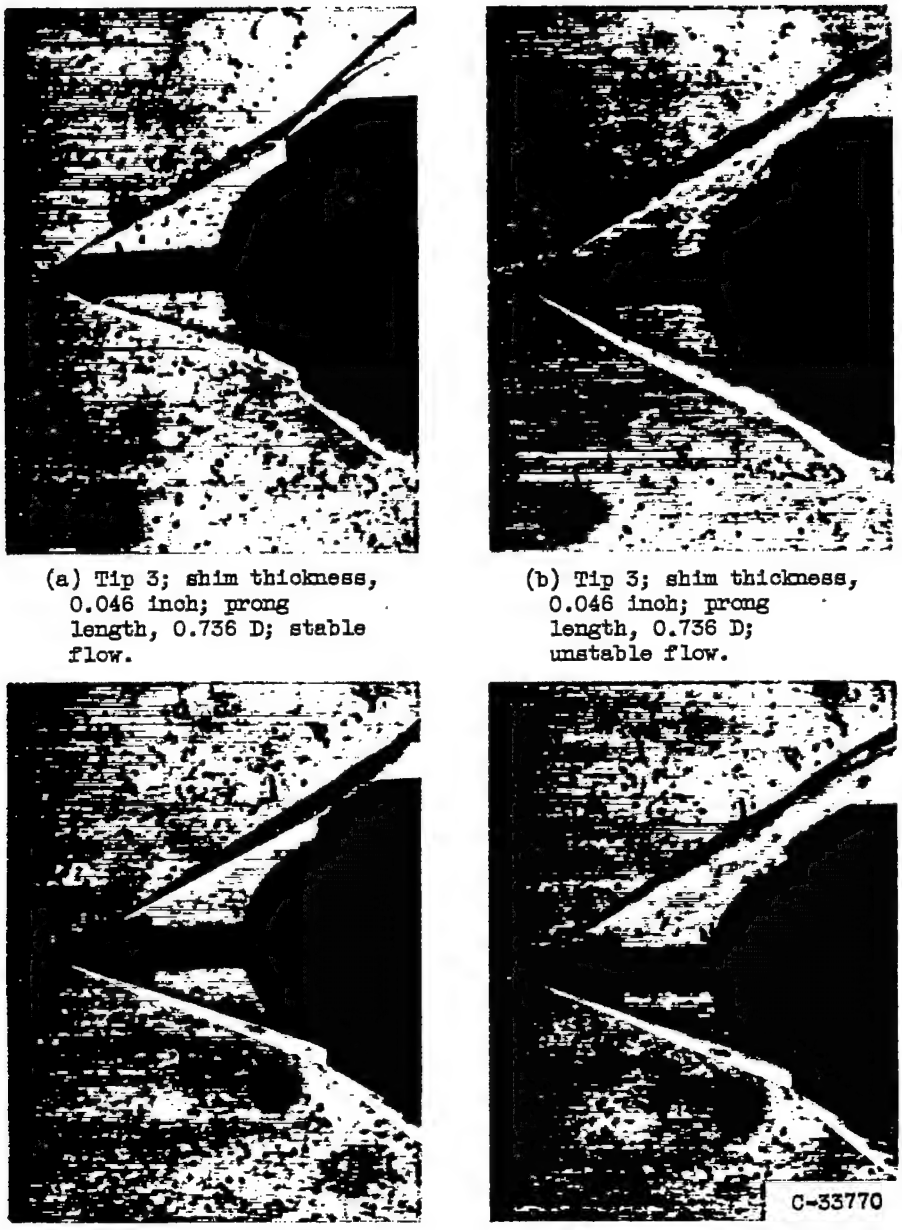

(a) Tip 3; shim thickness, 0.046 inch; prong length, 0.736 D; stable flow.

(b) Tip 3; shim thickness, 0.046 inch; prong length, 0.736 D; unstable flow.

(c) Tip 2; shim thickness, 0.056 inch; prong length, 0.834 D; stable flow.

(d) Tip 2; shim thickness, 0.056 inch; prong length, 0.834 D; unstable flow.

Figure 10. - Schlieren photographs of diffuser at 3° angle of attack. Spherical nose.

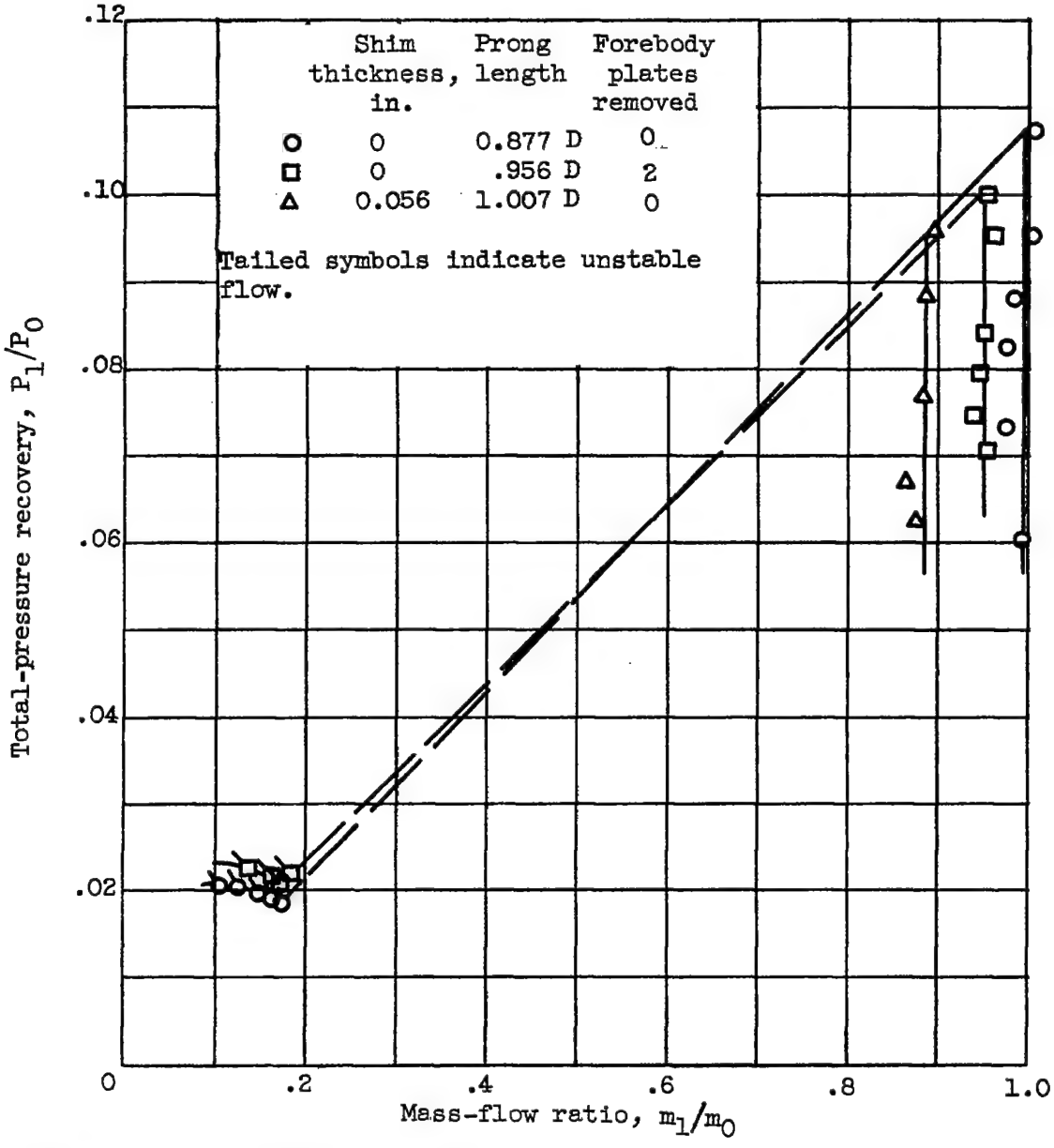

Figure 11. - Diffuser performance with planar-nose forebody. Tip 2; zero angle of attack.

(a) Two nose plates removed. Prong length, 0.956 D; stable flow.

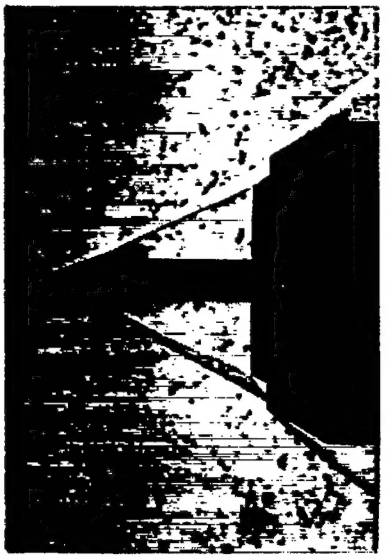

(b) All nose plates. Prong length, 0.877 D; stable flow.

(c) All nose plates. Prong length, 0.877 D; unstable flow.

(d) All nose plates. Prong length, 0.877 D; unstable flow.

Figure 12. - Schlieren photographs of diffuser at zero angle of attack. Tip 2; planar-nose forebody; no shim.

Figure 13. - Fluctuating flow ahead of spherical nose.

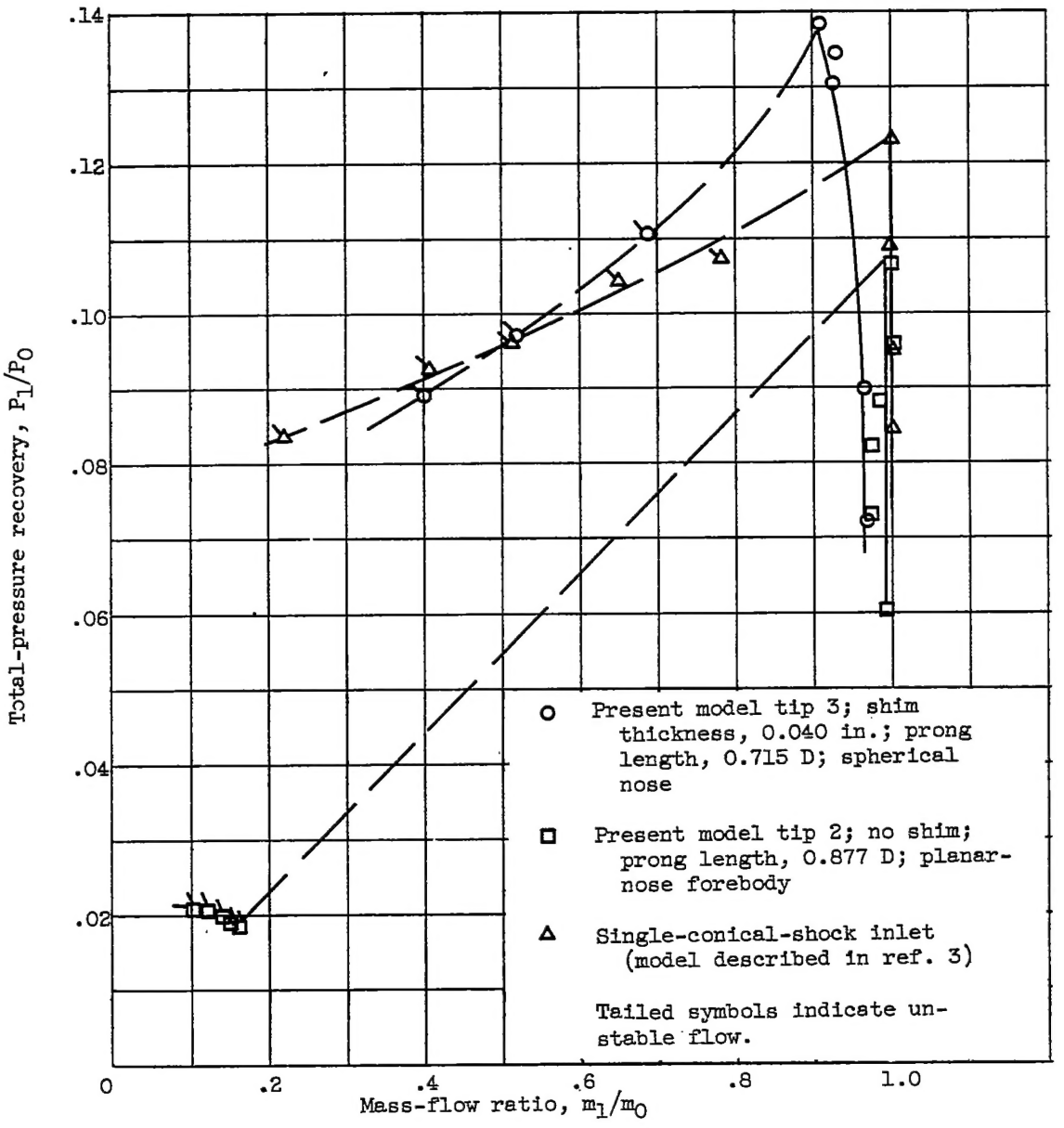

(a) Angle of attack, zero

Figure 14. - Comparison of diffuser characteristics.

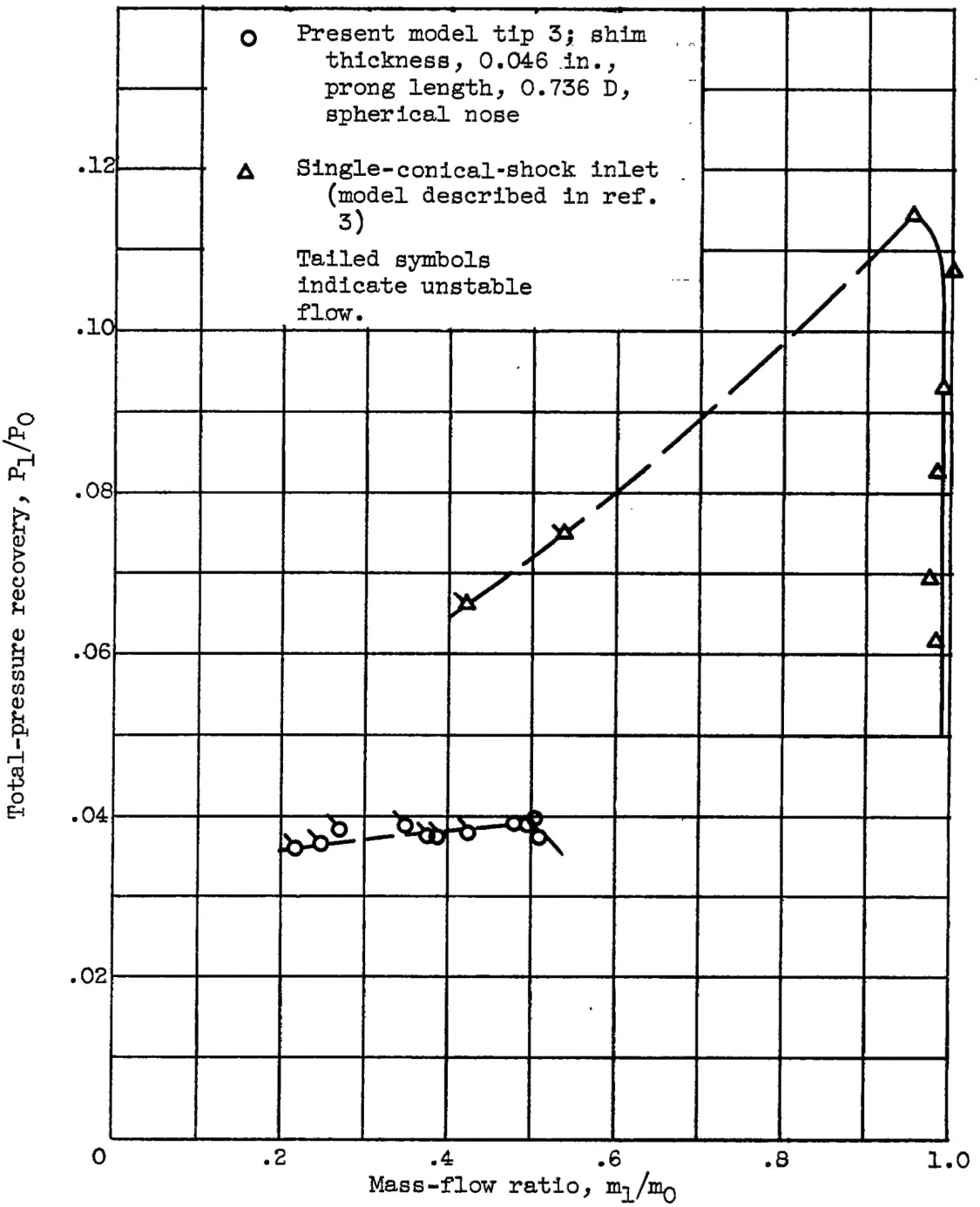

(b) Angle of attack, 3°.

Figure 14. - Concluded. Comparison of diffuser characteristics.

NACA-Langley - 12-1-53 - 325